JUSTC

Article

http://justc.ustc.edu.cn

Received: October 08, 2022; Accepted: January 01, 2023

Central electron-enriched NO-FeN_4 sites as superior acidic oxygen reduction reaction electrocatalysts for proton exchange membrane fuel cells

Cheng' an Zhong[1*], Tianpei Zhou[1,3*], Nan Zhang[2], Minglong Chen[1], Youxue Xie[1], Wensheng Yan[2], Wangsheng Chu[2], Xusheng Zheng[2], Qian Xu[2], Jiankai Ge[1], and Changzheng Wu[1,3] ✉

[1]*School of Chemistry and Materials Science, and CAS Center for Excellence in Nanoscience, University of Science and Technology of China, Hefei 230026, China;*
[2]*National Synchrotron Radiation Laboratory, University of Science and Technology of China, Hefei 230029, China;*
[3]*Institute of Energy, Hefei Comprehensive National Science Center, Hefei 230031, China*

* These authors contributed equally to this work
✉Correspondence: Changzheng Wu, E-mail: czwu@ustc.edu.cn

Graphical abstract

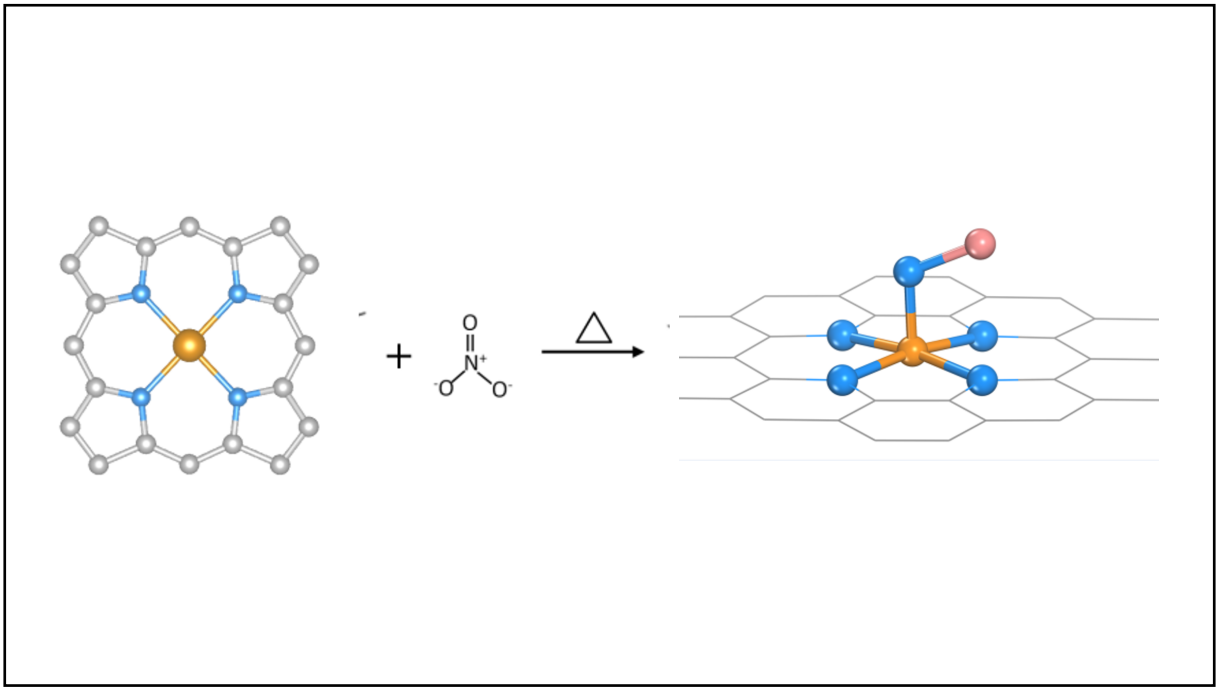

Restricted synthesis of new FeN_4 structures.

Public summary

- A central electron-enriched FeN_4 structure was established by the NO (nitrogen oxide) group directly modifying the Fe central, which exhibited three times higher mass activity compared to the traditional FeN_4 sample.
- The PEMFC assembled with the as-prepared electrocatalyst exhibits a much-enhanced peak power density (>725 $mW \cdot cm^{-2}$), providing a new approach to rationally designing advanced M-N_x nonnoble electrocatalysts for the oxygen reduction reaction.

Citation: Zhong C A, Zhou T P, Zhang N, et al. Central electron-enriched NO-FeN_4 sites as superior acidic oxygen reduction reaction electrocatalysts for proton exchange membrane fuel cells. *JUSTC*, **2023**, 53(3): 0304. DOI: 10.52396/JUSTC-2022-0143

JUSTC

Article

http://justc.ustc.edu.cn

Received: October 08, 2022; Accepted: January 01, 2023

Central electron-enriched NO-FeN_4 sites as superior acidic oxygen reduction reaction electrocatalysts for proton exchange membrane fuel cells

Cheng' an Zhong[1,*], Tianpei Zhou[1,3,*], Nan Zhang[2], Minglong Chen[1], Youxue Xie[1], Wensheng Yan[2], Wangsheng Chu[2], Xusheng Zheng[2], Qian Xu[2], Jiankai Ge[1], and Changzheng Wu[1,3] ✉

[1]*School of Chemistry and Materials Science, and CAS Center for Excellence in Nanoscience, University of Science and Technology of China, Hefei 230026, China;*
[2]*National Synchrotron Radiation Laboratory, University of Science and Technology of China, Hefei 230029, China;*
[3]*Institute of Energy, Hefei Comprehensive National Science Center, Hefei 230031, China*

* These authors contributed equally to this work
✉Correspondence: Changzheng Wu, E-mail: czwu@ustc.edu.cn

Cite This: *JUSTC*, **2023**, 53(3): 0304 (9pp) Read Online SI Supporting Information

Abstract: Developing nobel-metal-free catalysts, especially for iron-nitrogen on carbon (FeNC) materials, has been an urgent demand for wide applications of proton exchange membrane fuel cells (PEMFCs). However, the inferior oxygen reduction reaction (ORR) activity of traditional iron-nitrogen sites in acidic conditions seriously impedes the further improvement of their performance. Herein, we synthesized FeN_4 with NO (nitric oxide) group axial modification (denoted as NO-FeN_4) on a large scale through a confined small molecule synthesis strategy. Benefitting from the strong electron-withdrawing effect of the NO group, the central electron-rich FeN_4 site exhibits ultrahigh ORR activity with a three times higher mass activity (1.1 $A \cdot g^{-1}$ at 0.85 V) compared to the traditional FeN_4 sample, as well as full four-electron reaction selectivity. Moreover, the PEMFC assembled with the as-prepared electrocatalyst also exhibits a greatly enhanced peak power density (>725 $mW \cdot cm^{-2}$). This work provides a new approach to rationally design advanced M-N_x nonnoble electrocatalysts for the ORR.

Keywords: large-scale customization; oxygen reduction reaction; proton exchange membrane fuel cell; confined small molecule synthesis

CLC number: O643.36 **Document code:** A

1 Introduction

Proton exchange membrane fuel cells (PEMFCs) have been regarded as the most promising low-carbon energy conversion technology because of their amazing energy density, high efficiency, and environmental protection characteristics[1–3]. However, the sluggish oxygen reduction reaction largely impedes its wide application in PEMFC cathodes[4–5]. Noble metals with high activity, such as platinum, account for a high proportion of the cost of fuel cells, and this problem will become increasingly obvious with large-scale industrialization. Therefore, the development of nonprecious metal catalyst substitutes has become an important issue. Among many substitutes, atomically FeN_4 catalysts are favored by researchers due to their activity with promotion potential and low cost[6–8]. However, further requirements for selectivity and activity per unit are still driving the design and development of FeN_4 with new configurations.

FeN_4 with a conventional planar configuration has been studied as a potential cathode catalyst for PEMFCs for many years[9–11]. Nevertheless, this planar four-coordinate structure is easily attacked by protons or free radicals in acidic environments, causing leaching of iron ions in the FeN_4 site and oxidization of the surrounding carbon structure[12–13]. In addition, exposed Fe active centers are easily poisoned in the electrolyte solution, resulting in a decline in both stability and selectivity[14]. Therefore, effectively regulating the local coordination structure and electronic structure to obtain a new FeN_4 configuration arouses the extensive interest of researchers. For instance, most current reported regulation strategies are focused on heteroatom doping carbon substrates[15–16], fabricating carbon structure disorder[17], and introducing multiple active sites[18]. In these excellent works, it is worth noting that high-temperature thermal activation plays an important role in enhancing catalytic activity and stability. However, because high temperature greatly accelerates the diffusion of ions, the original structure of sites is often changed after thermal activation. Therefore, it is difficult to customize FeN_4 sites with a specific structure on a large scale[19–21].

Herein, by using confinement space and specific adsorption of NO to hemin, we developed an NO (nitrogen oxide) group axial-modified central electron-enriched FeN_4 structure (denoted as NO-FeN_4) with excellent ORR mass activity and selectivity for the first time. This specific FeN_4 site with a

DOI: 10.52396/JUSTC-2022-0143
JUSTC, **2023**, 53(3): 0304

modified electronic structure shows complete 4-electron reaction selectivity and high mass activity, which paves the way for designing advanced ORR electrocatalysts for PEMFCs.

2 Experiments

2.1 The synthesis of NO-FeN_4 product

All of the chemicals were of analytical grade and used without further purification. In a typical synthesis, 1 mmol hemin and 1 mmol $Zn(NO_3)_2$ were dissolved in 25 mL dimethylformamide under vigorous stirring for 30 min, and then 600 mg commercial activated carbon black (Ketjenblack EC600JD) and 25 mL dimethylformamide were snoicated for 1 h and dipped into the above solution. The mixed solution was continuously stirred for 4 h at 10 °C for adsorption until most of the hemin was adsorbed onto the carbon black. Then, the carbon black with adsorbed hemin/$Zn(NO_3)_2$ was separated from the mixture solution by washing with dimethylformamide several times, filtrating and freeze drying for 48 h. The obtained composite was directly pyrolyzed (at 650 °C for 2 h, heating rate of 10 °C·min^{-1}, in an Ar atmosphere). Then, the pyrolyzed product was leached in 0.5 mol·L^{-1} H_2SO_4 at 80 °C for 8 h to remove inactive iron and zinc species. The leached sample was washed to neutral with water and alcohol several times and dried in vacuum at 60 °C overnight to generate the carbon-supported NO-FeN_4 catalyst. For comparison, carbon black with only adsorbed hemin was also prepared under similar conditions, and the resultant sample was denoted as carbon black-supported FeN_4.

2.2 Fabrication of the working electrode for ORR catalytic activity testing

To prepare the working electrode, 4 mg catalysts mixed with 40 μL Nafion solution (Sigma Aldrich, 5 wt%) were dispersed into 1 mL isopropanol and water mixture solution (volume ratio 3∶1) and sonicated for at least 60 min to form a homogeneous catalyst ink. A certain volume of catalyst ink was then drop-cast onto the glassy carbon electrode with a 0.6 mg·cm^{-2} loading for all samples.

2.3 Fabrication of single PEMFC battery

The catalyst inks were prepared by using catalyst, isopropanol, deionized water and Nafion solution (Sigma Aldrich, 5 wt%) with a weight ratio of 1/90/30/11. The catalyst inks were ultrasonicated for 1 h and then brushed on carbon paper with an effective area of 5 cm^2 until the loading reached 4 mg·cm^{-2}. With a similar preparation process, commercial Pt/C (20 wt%) ink was dispersed on carbon paper with a loading of 0.2 mg Pt cm^{-2} as the anode. Using a thermocompressor, the prepared cathode and anode were then pressed onto the two sides of a Nafion 211 membrane (DuPont) at 130 °C and 5 MPa for 5 min to fabricate membrane electrode assemblies (MEAs). The MEA was measured in a single-cell and condition-controlled fuel cell test station (Scribner 850e, Scribner Associates). The flow rates of H_2 and O_2 were both 400 mL·min^{-1}, and the relative humidity was 100% during the PEFMC tests. During the test, the cell and input fuel temperature were maintained at 80 °C, and the back pressure was set at 0.2 MPa.

3 Results and discussion

3.1 Coordination structure analysis of central electron-enriched NO-FeN_4 sites

In this work, central electron-enriched NO-FeN_4 sites with optimized electronic configurations were prepared by adsorption of hemin and zinc nitrate into the mesopores of carbon black (Ketjenblack EC600JD) and rapid heat treatment. Through in situ mass spectrometry, we found that nitrate can rapidly generate a large number of nitric oxide groups (NO) with 650 °C fast pyrolysis treatment, and the generated NO groups tend to adsorb onto the central atom of porphyrin iron[22] (Supporting information Fig. S1a). In contrast, in Fig. S1b, nitric oxide cannot be detected at 30 *m/z* for FeN_4 precursors without adding nitrate (denoted as FeN_4). The detailed structural features of the as-prepared NO-FeN_4 electrocatalysts were investigated by X-ray diffraction (XRD) and Raman spectroscopy. As shown in Figs. S2 and S3**,** both NO-FeN_4 and FeN_4 show only two distinct peaks at approximately 26.2° and 43.2°, which could be ascribed to the characteristic (002) and (100) planes of graphitic carbon[23]. Meanwhile, the Raman spectra of the NO-FeN_4 and FeN_4 samples (Fig. S4) also display similar D-band (1326 cm^{-1}) for lattice defects and G-band (1585 cm^{-1}) for sp^2 hybrid carbon atoms. Additionally, the I_G/I_D ratios of NO-FeN_4 and FeN_4 were 0.81 and 0.83, respectively, indicating the similar graphitization degrees of the two catalysts[24]. These results suggest that no obvious Fe-based compounds exist in either the NO-FeN_4 or FeN_4 electrocatalysts. Moreover, the morphology and microstructure were also investigated by transmission and scanning electron microscopy. As shown in Figs. 1b and S5**,** the NO-FeN_4 electrocatalyst displays a spherical porous carbon structure, and no obvious nanoparticles could be found, indicating that the Fe atoms might be confined in carbon pores in atomically dispersed forms. Further investigation by high-angle annular dark field scanning transmission electron microscopy (HAADF-STEM) in Fig. 1c showed that many bright spots were homogeneously distributed in the porous carbon framework, confirming the atomically dispersed FeN_4 sites existing in the NO-FeN_4 sample. The corresponding energy-dispersive spectroscopy (EDS) mapping (Fig. 1d) shows that only Fe, N, and C are uniformly dispersed in the carbon framework, and no Zn can be detected, indicating that Zn has little residue after the wash and heat treatment processes. This conclusion can also be confirmed by X-ray photoelectron spectroscopy (XPS) analysis in Fig. S6. Similarly, FeN_4 samples prepared without confined NO treatment, which are denoted as FeN_4, are also presented in Figs. S1a, S3–4, S6, and S8–9. After systematic characterizations, the traditional FeN_4 sample seems to have similar features to NO-FeN_4 in terms of phase composition, morphology structure, and element distributions. Thus, it can be easily concluded that confined small molecule synthesis has no obvious effect on morphology and element distributions and that Fe atoms might form as single FeN_4 sites or clusters in the NO-FeN_4 sample. The detailed carbon structure was also investigated to exclude its influence on catalyst performance. Brunauer-Emmett-Teller (BET) analysis was also presented to analyze the

DOI: 10.52396/JUSTC-2022-0143
JUSTC, **2023**, 53(3): 0304

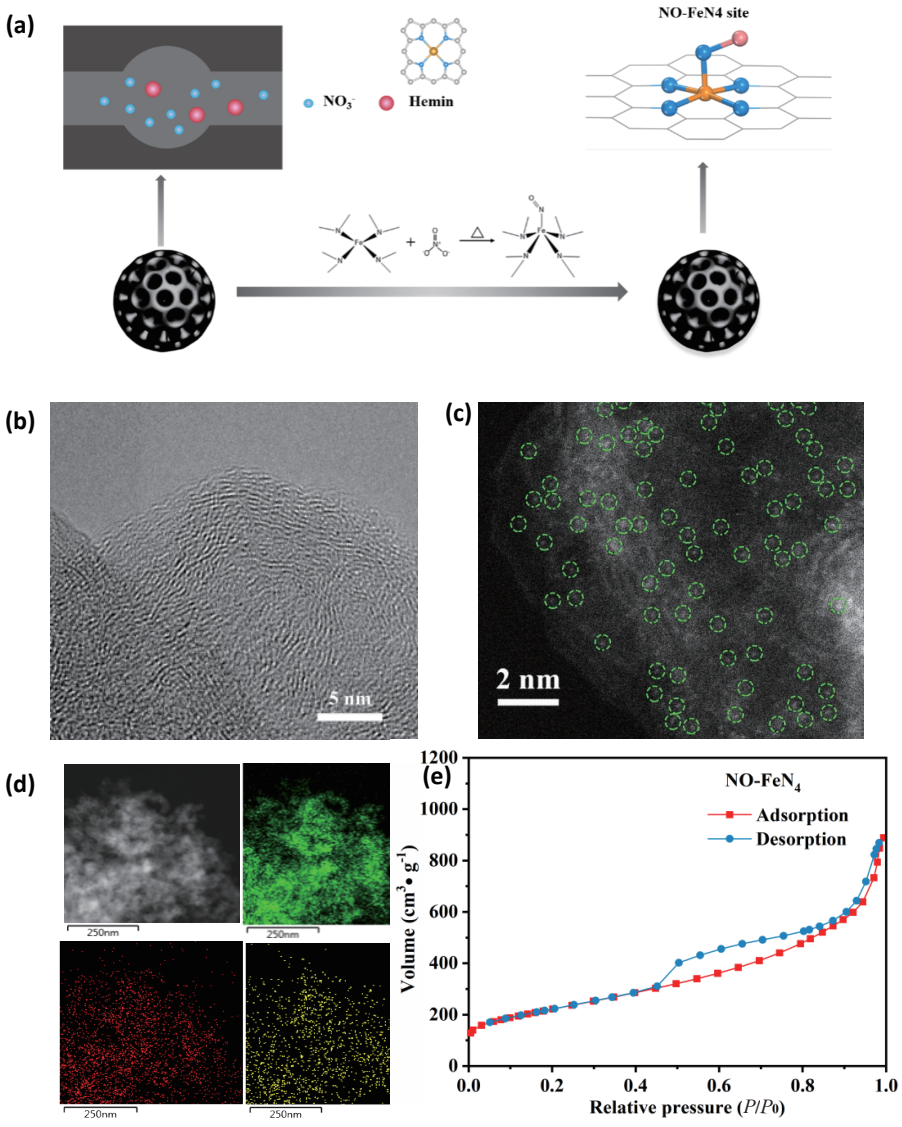

Fig. 1. (a) Schematic representation of the synthesis for NO-FeN_4. (b) HRTEM images of NO-FeN_4 material. (c) HAADF-STEM images of NO-FeN_4. (d) Elemental mapping images for the NO-FeN_4. (e) N_2 adsorption/desorption isotherms and corresponding pore size distribution curves (inset) of as-prepared NO-FeN_4 product.

BET surface area and pore size distribution of NO-FeN_4 and its contrast. In Fig. 1e, NO-FeN_4 exhibits a surface area of 760.7 $m^2 \cdot g^{-1}$, which is comparable to that of the FeN_4 sample (794.5 $m^2 \cdot g^{-1}$). In addition, the isotherm hysteresis loops of the NO-FeN_4 and FeN_4 samples exhibit obvious type-IV isotherms, indicating the same mesoporous carbon configuration of the two catalysts[25]. Moreover, the corresponding pore size distribution also confirms that these two catalysts both have a large number of mesopores with a diameter of approximately 3.2 nm (Fig. 1e inset). Comprehensive analysis of the results above, it can be concluded that NO-FeN_4 catalysts have no significant difference in phase, element composition, morphology or detailed carbon structure properties. Therefore, the specific modified FeN_4 sites might play a key role in enhancing ORR activities.

To evaluate the local atomic structure around the NO-FeN_4 catalyst, X-ray absorption structure (XAS) measurements were performed. As shown in Fig. 2a and b, the XANES spectra of both the NO-FeN_4 and FeN_4 samples present similar preedge peaks at 7113.6 eV compared with the standard hemin precursor, suggesting their similar main structure of a typical square-planar Fe-N_4 structure (D_{4h} symmetry)[26]. However, the negative energy shifting of the absorption edge (Fig. 2c), as well as the lower white-line intensity (Fig. 2b) of NO-FeN_4, suggests that its 3d orbital electron density is higher than that of the FeN_4 sample, which means that the enrichment of d-electrons in the Fe center of NO-FeN_4 catalysts occurs[27]. Moreover, an in-depth investigation of NO-FeN_4 was also performed, as shown in Fig. 2d. From Fourier transform (FT) plots of the Fe K-edge results in R-space, NO-FeN_4 presented one main peak at 1.51 Å, which was considered to be an elongated Fe-N shell compared with the FeN_4 sample at 1.48 Å. To further reveal the local coordination structure of Fe atoms, Fe K-edge EXAFS spectra of NO-FeN_4 and FeN_4 catalysts were both fitted. As shown in Fig. S10, NO-FeN_4 exhibited an Fe–N/O bond length of 2.03 Å ± 0.03 Å with a N/O coordination number of 5.6 ± 0.6, which is different from that of the FeN_4 sample (2.00 Å ± 0.03 Å, 6.4 ± 0.6),

DOI: 10.52396/JUSTC-2022-0143
JUSTC, **2023**, 53(3): 0304

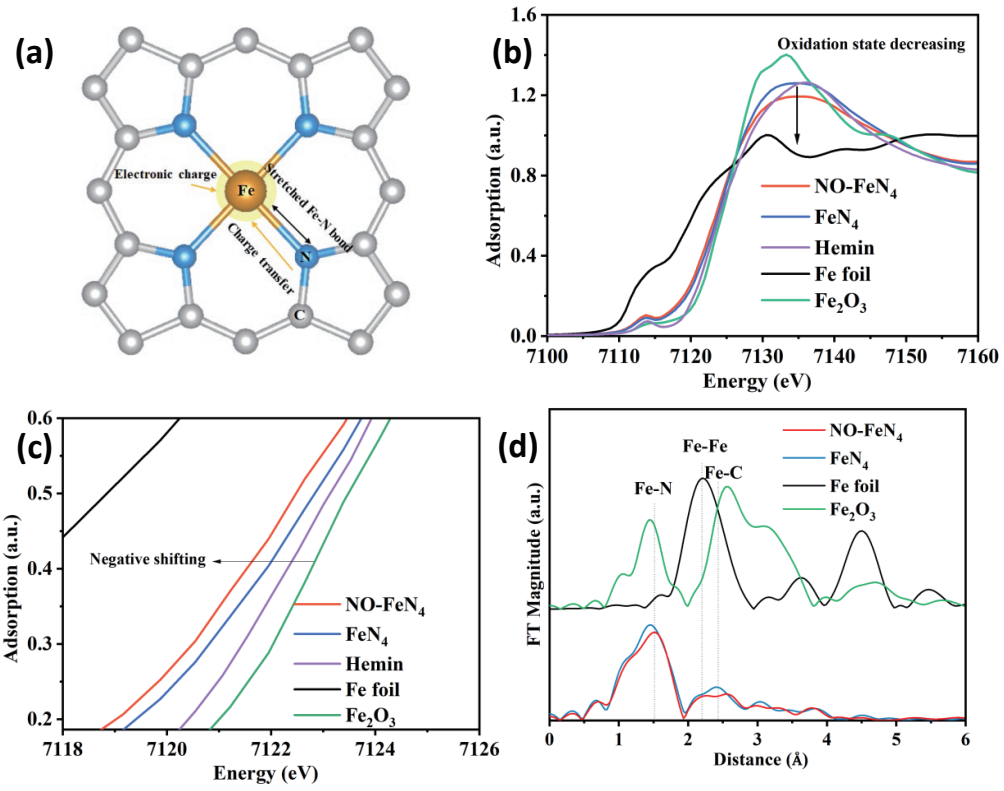

Fig. 2. (a) Schematic illustration of electronic structure for NO-FeN$_4$. (b) and (c) Fe K-edge X-ray absorption near edge structures (XANES). (d) The Fe K-edge extended XAFS oscillation function of NO-FeN$_4$ and FeN$_4$ samples.

demonstrating that increased Fe–N/O bond length has an obvious effect on the coordination number of Fe center atoms, which might change the adsorption/desorption energy of reactants. Based on the XAFS results, NO-FeN$_4$ has a larger bond length than FeN$_4$, which provides the opportunity to discuss the structure-function relationship between the bond length and the catalytic activity. As is well known, the metal iron center can act as an oxygen molecule adsorption center during the ORR process[26]. Therefore, the intrinsic ORR catalytic activity of the FeN$_4$ materials is highly dependent on the nature of the Fe center. In fact, due to the stretched Fe–N bond length, NO-FeN$_4$ with an electron-rich Fe atom center could suppress the Fe-to-ligand back-donation between the Fe atom center and its adsorbed oxygen species, causing enhancement of the $Fe^{2+/3+}$ redox potential and reducing site-blocking effects on the ORR[28]. As far as we know, the scaled customization of the FeN$_4$ structure in the high-temperature pyrolysis process is still a great challenge. As shown in Fig. S11**,** the NO-FeN$_4$ site can be customized on a large scale during the pyrolysis process owing to the confinement space and specific adsorption of NO to hemin.

3.2 Electron structure analysis of central electron-enriched NO-FeN$_4$ sites

It has been widely recognized that the NO group has a strong electron absorption effect[29], while the electronic structure and valence state around the Fe center have been systematically studied by soft X-ray absorption near-edge spectroscopy (XANES) and X-ray photoelectron spectroscopic (XPS) analysis. As shown in Fig. 3a, the normalized XANES spectrum of NO-FeN$_4$ at the Fe L$_3$ edge has a lower peak intensity and a negative energy shift compared to that of the FeN$_4$ electrocatalyst, indicating that more electrons occupy the Fe 3d orbitals of NO-FeN$_4$, which is consistent with the Fe K-edge result above. Moreover, in Fig. 3b, the C K-edge XANES spectra of the NO-FeN$_4$ and FeN$_4$ products exhibit a δ*C–C transition centered at ~303.5 eV and a π*C=C transition at ~295.6 eV, which represent typical sp^2-hybridized carbon[30]. The increased π*C=C intensity for NO-FeN$_4$ suggests that it has fewer electrons in the C 2p orbitals than FeN$_4$. This phenomenon hints that more electrons might flow into the Fe center of NO-FeN$_4$, demonstrating a stronger charge transfer effect. In addition, N K-edge XANES and XPS spectra can also verify the findings discovered above. As shown in Fig. 3c, the N K-edge of NO-FeN$_4$ represents two typical spectroscopic features: the 1s→π* transition in the region of 393.0–401.0 eV and the 1s→σ* transition at 401.0–410.0 eV. Specifically, peak **a** can be ascribed to the π* transition of Fe-bonded pyrrole-type N at 398.5 eV, and **b** can be assigned to the π* transition of graphitic-type N-groups at 401.5 eV[31]. Notably, peak **a** of NO-FeN$_4$ exhibits lower absorption intensity in the two resonances. This result suggests that the formation of the Fe−N−C chemical bond in NO-FeN$_4$ has a stronger charge transfer effect. Furthermore, in Fig. 3d, the X-ray photoelectron spectroscopy (XPS) spectra of N 1s also reveal that the Fe-pyrrolic N peak in NO-FeN$_4$ shifts to a higher binding energy (399.1 eV) compared with FeN$_4$ materials (398.8 eV)[32]. In Fig. S12, the core-level scan spectrum of Fe 2p shows that the Fe 2p$^{3/2}$ peak of NO-FeN$_4$ has a slight negative shift compared with that of FeN$_4$. These results confirm that a faster electron transfer pathway has formed between the Fe center

DOI: 10.52396/JUSTC-2022-0143
JUSTC, **2023**, 53(3): 0304

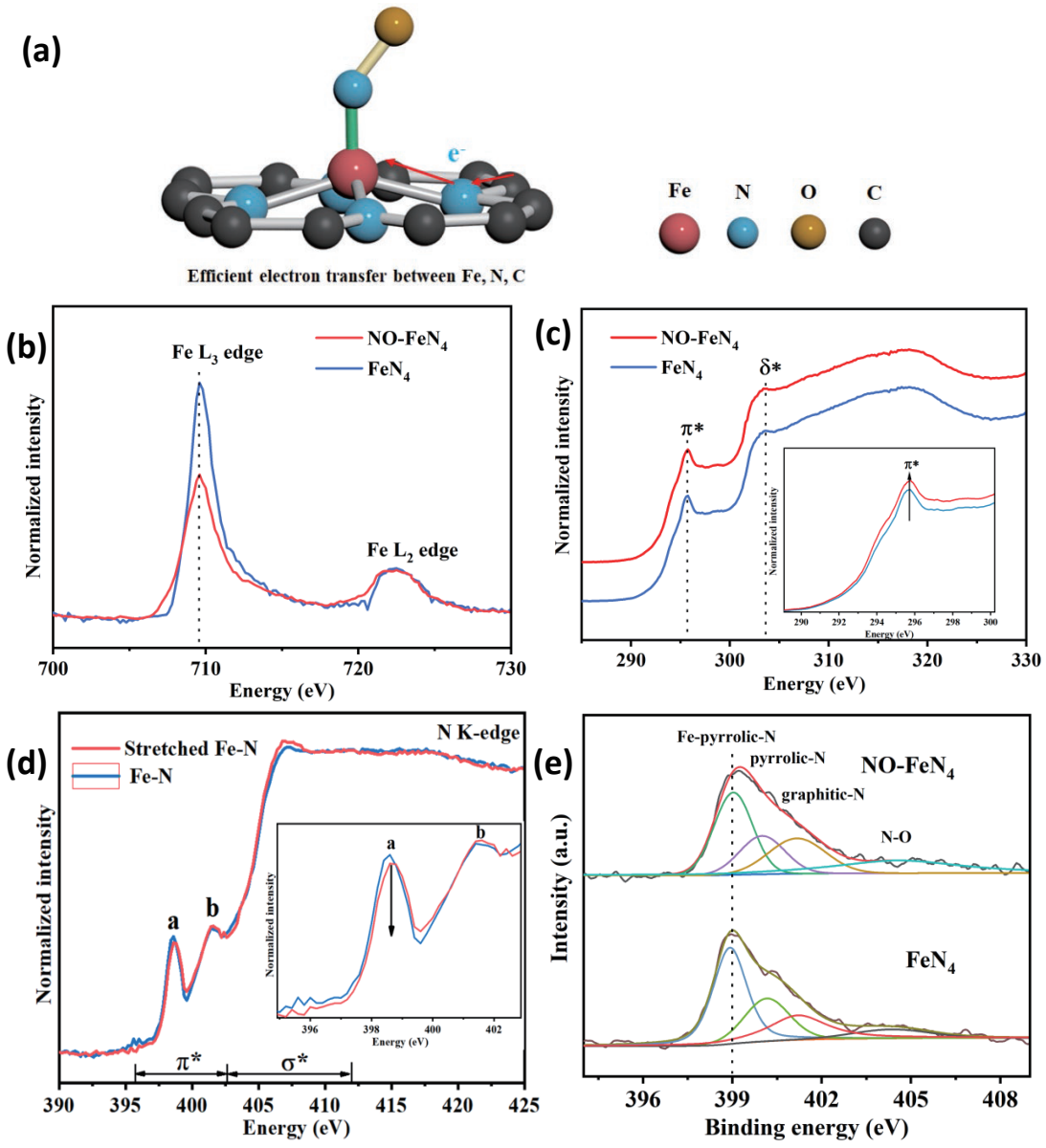

Fig. 3. (a) Electron transfer diagram of N, C adjacent to Fe central of NO-FeN_4. (b) Soft-XAS spectra of Fe L-edge, (c) C K-edge and (d) N K-edge of NO-FeN_4 and FeN_4. (e) XPS spectra of N 1s of NO-FeN_4.

and its substrate due to the strong electron absorption effect of NO. This suggests establishing a fast electron transport pathway between the substrate and the active sites.

To verify the ORR activity of the NO-FeN_4 and FeN_4 electrocatalysts, rotating ring-disk electrode (RRDE) measurements were first performed in an acidic medium. As shown in Fig. 4a, the linear scan sweep voltammetry (LSV) curves exhibited a positive onset potential of 0.90 V and a half-wave potential of 0.82 V for NO-FeN_4, which is much higher than that of the FeN_4 electrocatalyst (0.75 V) and close to that of commercial Pt/C. To quantitatively evaluate the ORR activity of the as-prepared NO-FeN_4 sample, Tafel slopes and electrochemical impedance spectroscopy (EIS) were also performed, as shown in Fig. 4b and Fig. S13. NO-FeN_4 has a relatively small Tafel slope value (77 mV/dec) compared to that of FeN_4 (90 mV/dec) and Pt/C (110 mV/dec). Moreover, it also shows the smallest semicircle, which represents the minimum interface charge transfer resistance, indicating the extremely high kinetic activity for the NO-FeN_4 sample. In Fig. 4c, the mass activity at 0.85 V was also calculated to demonstrate the high catalytic activity of the NO-FeN_4 sample. In Fig. 4d, NO-FeN_4 exhibits the largest mass activity of 9.3 $A \cdot g^{-1}$. Moreover, the turnover frequency (TOF) of NO-FeN_4 is 1.14 $e \cdot s^{-1} \cdot site^{-1}$. It is 1.375 times that of the FeN_4 sample, indicating that the Fe–N bond length endows its ultrahigh intrinsic activity. Moreover, the peroxide (H_2O_2) generation percent and electron transfer number were also evaluated using the RRDE technique. As shown in Fig. 4d, NO-FeN_4 exhibited a relatively low H_2O_2 yield ranging from 1.3% to 1.8%, and the corresponding electron transfer number exceeded 3.97 below 0.8 V, suggesting its high selectivity and a direct four-electron pathway. These results revealed that NO-FeN_4 could suppress the generation of H_2O_2 and reduce the Fenton reaction during the ORR process. As shown in Fig. 4e,

DOI: 10.52396/JUSTC-2022-0143
JUSTC, **2023**, 53(3): 0304

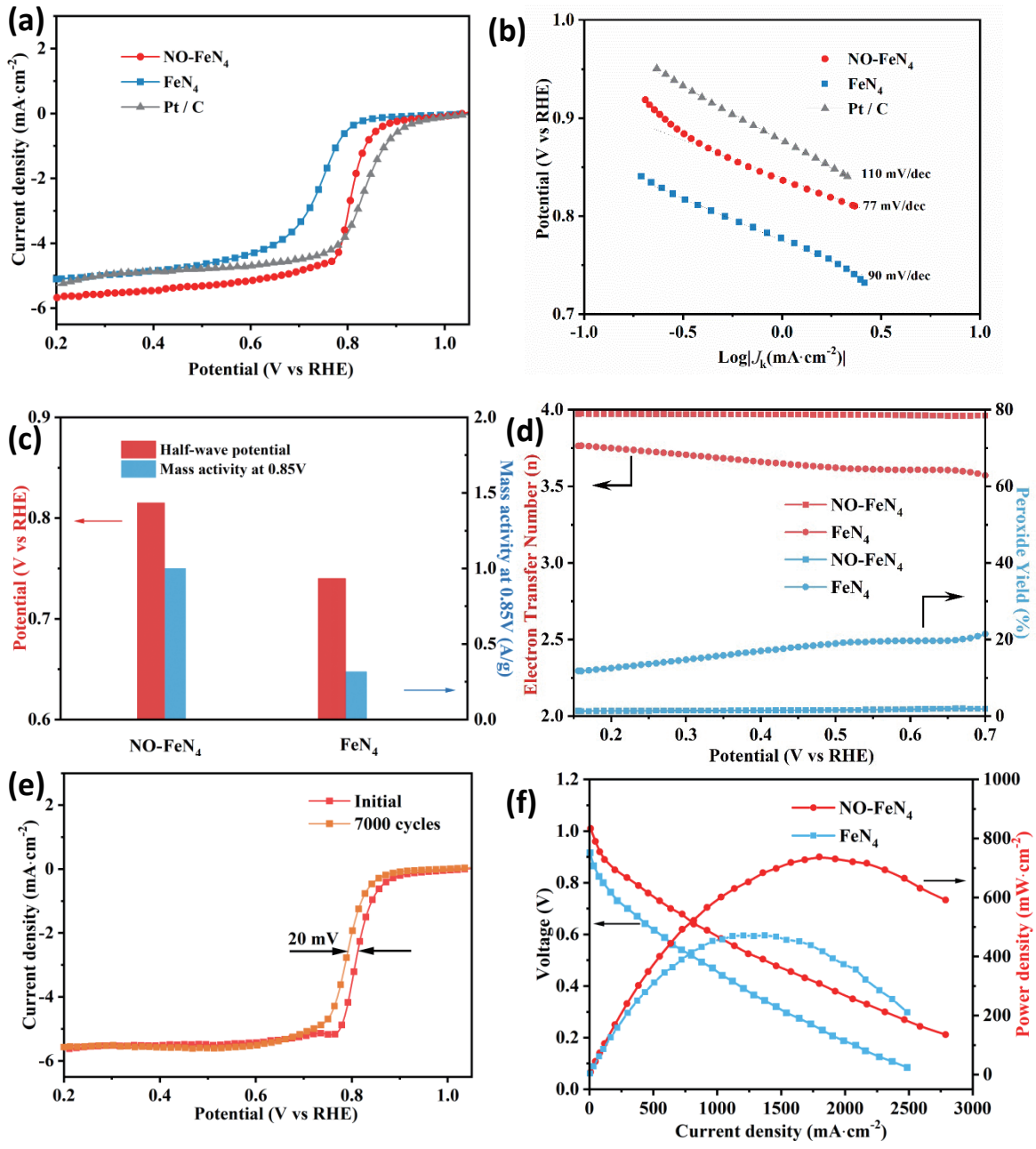

Fig. 4. Electrocatalytic performance. (a) ORR polarization curves and (b) corresponding Tafel plots of NO-FeN$_4$ and FeN$_4$ in O$_2$-saturated 0.5 mol·L^{-1} H$_2$SO$_4$ and 20% Pt/C in 0.1 mol·L^{-1} HClO$_4$ under a rotating rate of 1600 r·min^{-1}. (c) Comparison of mass activity at 0.85 V and half-wave potential of NO-FeN$_4$ and FeN$_4$ catalysts. (d) Peroxide yield and electron transfer number of NO-FeN$_4$ and FeN$_4$ sample during ORR process. (e) LSV curves of NO-FeN$_4$ catalysts before and after 7000 CV cycles. (f) Polarization and power density curves of NO-FeN$_4$ and FeN$_4$ based membrane electrode assemblies in PEMFCs. Cell temperature: 80 ℃; RH: 100%, H$_2$/O$_2$: 1.5 bar.

only a 20 mV loss can be detected after 7000 CV cycles for NO-FeN$_4$ in O$_2$-saturated 0.5 mol·L^{-1} H$_2$SO$_4$. However, the half-wave potential of the FeN$_4$ sample decreased by 47 mV under the same conditions (Fig. S14). These results prove that NO-FeN$_4$ exhibits significantly enhanced catalytic activity as well as stability and could be a promising cathode electrocatalyst for PEMFCs. The excellent ORR activity of the NO-FeN$_4$ sample was also demonstrated by integrating it into membrane-electrode assemblies (MEAs) with a total catalyst loading of 4.0 mg·cm^{-2} for PEMFC testing. As shown in Fig. 4f, under the test condition of 1.5 bar H$_2$/O$_2$ back pressure, the NO-FeN$_4$ exhibited an open-circuit potential of 1.01 V and generated a current density of 355 mA·cm^{-2} at 0.8 V and 1828 mA·cm^{-2} at 0.4 V, which surpasses the FeN$_4$ catalyst. Moreover, the corresponding peak power density of NO-FeN$_4$ reached 735 mW·cm^{-2}, which was much higher than that of FeN$_4$ (481 mW·cm^{-2}), indicating its broad application prospects in PEMFCs.

The specific reaction mechanism of NO-FeN$_4$ was further investigated by operando XAFS tests. As shown in Fig. 5a,

DOI: 10.52396/JUSTC-2022-0143
JUSTC, **2023**, 53(3): 0304

operando XAS tests were conducted on a three-electrode system by using a gas diffusion electrode composited with NO-FeN_4 as a cathode in fluorescence mode. In Fig. 5b, the first derivative of the XANES spectra of NO-FeN_4 at the open circuit exhibited obvious positive energy shifting compared to the dry powder sample, indicating that the adsorption of oxygen species in the electrolyte may lead to an increase in the oxidation state for central Fe atoms, while excessive impurity adsorption in the electrolyte may be harmful to the fast oxygen reduction reaction FeN_4 sites. Additionally, Fig. 5c shows the normalized XANES spectra of the Fe K-edge for NO-FeN_4, and the adsorption edge exhibited negative shifting along with the decrease in applied potential, indicating that the ORR is closely related to the Fe^{2+}/Fe^{3+} redox potential. Notably, the adsorption edge of 1.0 V and 1.0 V after cycles coincide, which proves that NO-FeN_4 has good cycle stability. As the adsorption of reactants at FeN_4 sites plays a key role in the ORR process, a surface-sensitive delta-mu (Δμ) technique in the X-ray absorption near-edge spectra (XANES) region was used to study the adsorption state of reactants at the NO-FeN_4 sites. For example, in 0.5 mol·L^{-1} H_2SO_4, the experimental Δμ spectrum is obtained by subtracting the region of the Fe K-edge at 0.1 and 1.0 V (or 0.9, 0.7, and 0.3 V). As shown in Fig. 5d, the corresponding Δμ-XANES also shows that NO-FeN_4 exhibited a significant increase in |Δμ| between 0.7 and 0.9 V, which means that it could decompose adsorbed oxygen molecules at a relatively high potential, avoid the influence of adsorbed impurities, and improve the ORR activity[33]. Since most FeN_4 catalysts are easily poisoned by impurities at the beginning of the reaction process, a low reaction potential is required to decompose impurities and conduct an oxygen reduction reaction. Therefore, the high reaction potential of NO-FeN_4 indicates that it is not easily poisoned, leading to a higher reaction activity and stability. In conclusion, all the above results demonstrate that NO-FeN_4 exhibits accelerated kinetics and relatively high stability for oxygen reduction under acidic conditions.

The much-enhanced ORR performance of NO-FeN_4 can be ascribed to the following features: (i) the highly dispersed FeN_4 sites could significantly improve ORR catalytic activity. (ii) Δμ-XANES analysis shows that NO-FeN_4 sites possess highly reversible Fe^{2+}/Fe^{3+} redox potential and are less likely to be affected by adsorbed impurities. (iii) Rapid electron transfer occurs between the Fe center and its coordinated nitrogen and carbon atoms, which greatly expedites the reduction process of adsorption oxygen species. (iv) The porous and highly graphitization carbon configuration increases the utilization and robust ability of electrocatalysts. Benefiting from the combination of highly active sites and open exposure areas, NO-FeN_4 exhibits superior ORR catalytic activity in an acidic medium as well as high power density when integrated into PEMFC systems.

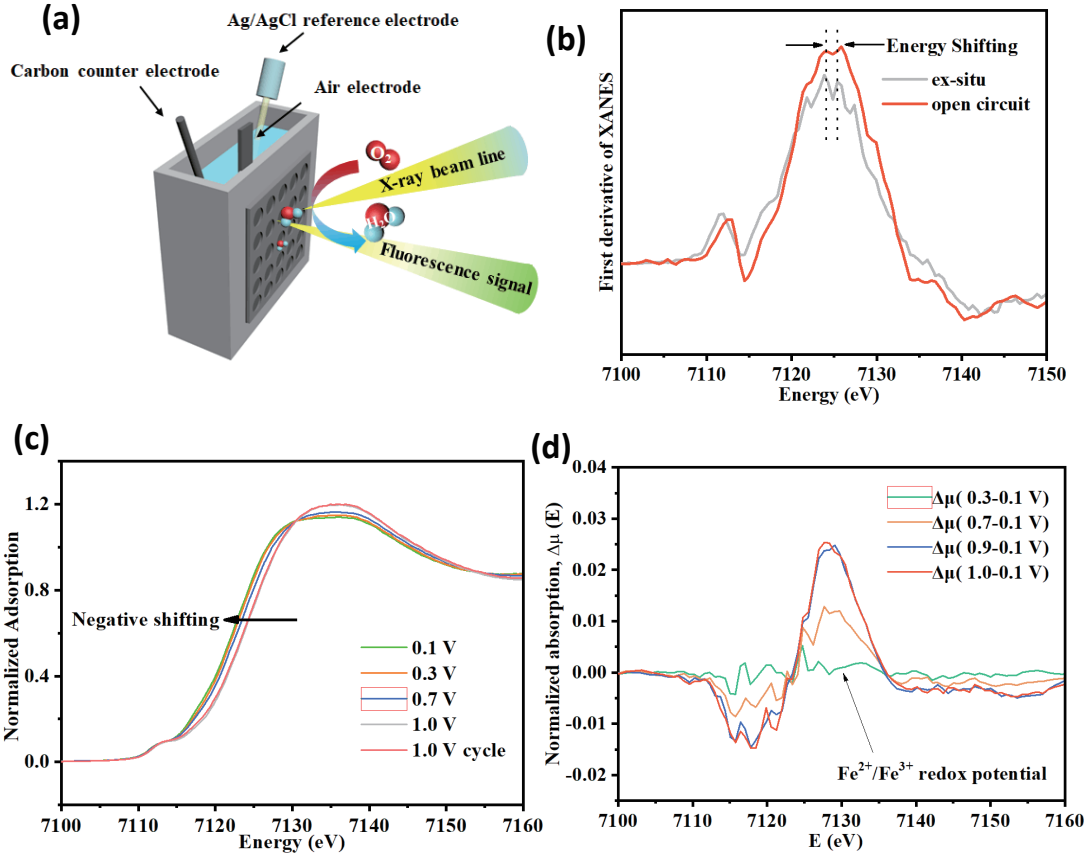

Fig. 5. (a) Schematic of operando XAS measurement device and three-electrode half-cell. (b) First derivative of XANES spectra of NO-FeN_4 for dry powder and operando sample. (c) Operando XANES spectra of Fe K-edge for NO-FeN_4. (d) Normalized difference spectra for Fe K-edge of NO-FeN_4 at different potentials at operando condition.

DOI: 10.52396/JUSTC-2022-0143
JUSTC, **2023**, 53(3): 0304

4 Conclusions

In conclusion, the central electron-enriched NO-FeN$_4$ structure has been successfully developed as a high-efficiency cathode electrocatalyst. Because the confined small molecule modification significantly increases the charge densities of central iron atoms, the as-prepared electrocatalyst exhibits much enhanced intrinsic catalytic activity, fast electron transfer ability and full four-electron reaction selectivity. Moreover, the as-prepared NO-FeN$_4$ electrocatalyst shows high mass activity (1.1 A·g^{-1} at 0.85 V) and TOF activity (1.14 e·s^{-1}·site^{-1}), and its half-wave potential is also close to that of the commercial Pt/C sample. As a result, the PEMFC built by this electrocatalyst has a high power density of 725 mW·cm^{-2} at 80 °C, 1.5 bar back pressure, and 100% relative humidity, demonstrating its promising potential in practical applications. This work will pave new avenues for the design of advanced nonnoble electrocatalysts for PEMFCs.

Supporting information

The supporting information for this article can be found online at https://doi.org/10.52396/JUSTC-2022-0143. The supporting information includes an experimental section, XPS spectra, TEM images, N_2 physisorption isotherms, LSV curves, structural parameters, and electrochemical performances.

Acknowledgements

This work was financially supported by the Natural Science Foundation of China (21925110, 21890751, 91745113), the National Program for Support of Top-Notch Young Professionals, USTC Research Funds of the Double First-Class Initiative (YD2060002004), the Key R&D Program of Shandong Province (2021CXGC010302), the Major Program of Development Foundation of Hefei Center for Physical Science and Technology (2016FXZY001), the Users with Excellence Project of Hefei Science Center CAS (2021HSCUE004), the Strategic Priority Research Program of the Chinese Academy of Sciences (XDB36000000), and the Anhui Provincial Natural Science Foundation (1808085MB26). The authors also appreciate the support from the beamline 1W1B of Beijing Synchrotron Radiation Facility (BSRF, Beijing, China) and the beam-lines BL11U, BL10B, and BL12B-a of National Synchrotron Radiation Laboratory (NSRL, Hefei, China), the fellowship of China National Postdoctoral Program for Innovative Talents (BX2021280), and the fellowship of China Postdoctoral Science Foundation (2022M710141).

Conflict of interest

The authors declare that they have no conflict of interest.

Biographies

Cheng' an Zhong is currently a master' s student at the School of Chemistry and Materials Science, University of Science and Technology of China, under the supervision of Prof. Changzheng Wu. His research mainly focuses on FeN$_4$ oxygen reduction catalysts, zinc air batteries, and fuel cells.

Tianpei Zhou is currently a postdoctoral researcher at the School of Chemistry and Materials Science, University of Science and Technology of China. His research mainly focuses on oxygen reduction catalysts, zinc air batteries, fuel cells and thermal insulation material.

Changzheng Wu received his Ph.D. degree from the University of Science and Technology of China. He is currently a Professor at the University of Science and Technology of China. His research interests include preparation and characterization of two-dimensional materials, oxygen reduction catalysts and fuel cells, relevant mechanism and functional application of transition metal oxide and sulfide strongly correlated system materials.

References

[1] Xiao F, Wang Y C, Wu Z P, et al. Recent advances in electrocatalysts for proton exchange membrane fuel cells and alkaline membrane fuel cells. *Adv. Mater.*, **2021**, *33*: 2006292.

[2] Jiao K, Xuan J, Du Q, et al. Designing the next generation of proton-exchange membrane fuel cells. *Nature,* **2021**, *595*: 361–369.

[3] Debe M K. Electrocatalyst approaches and challenges for automotive fuel cells. *Nature,* **2012**, *486*: 43–51.

[4] Martinez U, Komini Babu S, Holby E F, et al. Progress in the development of Fe-based PGM-free electrocatalysts for the oxygen reduction reaction. *Adv. Mater.*, **2019**, *31*: 1806545.

[5] Shao M, Chang Q, Dodelet J P, et al. Recent advances in electrocatalysts for oxygen reduction reaction. *Chem. Rev.*, **2016**, *116*: 3594–3657.

[6] Lefèvre M, Proietti E, Jaouen F, et al. Iron-based catalysts with improved oxygen reduction activity in polymer electrolyte fuel cells. *Science,* **2009**, *324*: 71–74.

[7] Jiang W J, Gu L, Li L, et al. Understanding the high activity of Fe-N-C electrocatalysts in oxygen reduction: Fe/Fe$_3$C nanoparticles boost the activity of Fe-N$_x$. *J. Am. Chem. Soc.*, **2016**, *138*: 3570–3578.

[8] Sa Y J, Seo D J, Woo J, et al. General approach to preferential formation of active Fe-N$_x$ Sites in Fe-N/C electrocatalysts for efficient oxygen reduction reaction. *J. Am. Chem. Soc.*, **2016**, *138*: 15046–15056.

[9] Chung H T, Cullen D A, Higgins D, et al. Direct atomic-level insight into the active sites of a high-performance PGM-free ORR catalyst. *Science,* **2017**, *357*: 479–484.

[10] Lefèvre M, Dodelet J P. Fe-based catalysts for the reduction of oxygen in polymer electrolyte membrane fuel cell conditions: Determination of the amount of peroxide released during electroreduction and its influence on the stability of the catalysts. *Electrochim. Acta,* **2003**, *48*: 2749–2760.

[11] Kramm U I, Herrmann-Geppert I, Behrends J, et al. On an easy way to prepare metal nitrogen doped carbon with exclusive presence of MeN$_4$-type sites active for the ORR. *J. Am. Chem. Soc.*, **2016**, *138*: 635–640.

[12] Jia Q Y, Ramaswamy N, Tylus U, et al. Spectroscopic insights into the nature of active sites in iron-nitrogen-carbon electrocatalysts for oxygen reduction in acid. *Nano Energy,* **2016**, *29*: 65–82.

[13] Bae G, Chung M W, Ji S G, et al. PH effect on the H_2O_2-induced deactivation of Fe-N-C catalysts. *ACS Catal.*, **2020**, *10*: 8485–8495.

[14] Gupta S, Zhao S, Ogoke O, et al. Engineering favorable morphology and structure of Fe-N-C oxygen-reduction catalysts through tuning of nitrogen/carbon precursors. *ChemSusChem,* **2017**, *10*: 774–785.

[15] Wang Y C, Lai Y J, Song L, et al. S-doping of an Fe/N/C ORR catalyst for polymer electrolyte membrane fuel cells with high power density. *Angew. Chem. Int. Ed.*, **2015**, *54*: 9907–9910.

DOI: 10.52396/JUSTC-2022-0143
JUSTC, **2023**, 53(3): 0304

[16] Ni B X, Chen R, Wu L M, et al. Optimized enhancement effect of sulfur in Fe-N-S codoped carbon nanosheets for efficient oxygen reduction reaction. *ACS Appl. Mater. Inter.,* **2020**, *12*: 23995–24006.
[17] Dipojono H K, Saputro A G, Fajrial A K, et al. Oxygen reduction reaction mechanism on a phosporus-doped pyrolyzed graphitic Fe/N/C catalyst. *New J. Chem.,* **2019**, *43*: 11408–11418.
[18] Lefèvre M, Dodelet J P, Bertrand P. Molecular oxygen reduction in PEM fuel cells: Evidence for the simultaneous presence of two active sites in Fe-based catalysts. *J. Phys. Chem. B,* **2002**, *106*: 8705–8713.
[19] Zhang N, Zhou T P, Chen M L, et al. High-purity pyrrole-type FeN_4 sites as a superior oxygen reduction electrocatalyst. *Energ. Environ. Sci.,* **2020**, *13*: 111–118.
[20] Santoro C, Serov A, Gokhale R, et al. A family of Fe-N-C oxygen reduction electrocatalysts for microbial fuel cell (MFC) application: Relationships between surface chemistry and performances. *Appl. Catal. B-Environ,* **2017**, *205*: 24–33.
[21] Zitolo A, Goellner V, Armel V, et al. Identification of catalytic sites for oxygen reduction in iron- and nitrogen-doped graphene materials. *Nat. Mater.,* **2015**, *14*: 937–942.
[22] Kurihara H, Ohta A, Fujisawa K. Structures and properties of dinitrosyl iron and cobalt complexes ligated by bis(3, 5-diisopropyl-1-pyrazolyl)methane. *Inorganics,* **2019**, *7* (10): 116.
[23] Panomsuwan G, Saito N, Ishizaki T. Nitrogen-doped carbon nanoparticle-carbon nanofiber composite as an efficient metal-free cathode catalyst for oxygen reduction reaction. *ACS Appl. Mater. Inter.,* **2016**, *8*: 6962–6971.
[24] Yu H J, Shang L, Bian T, et al. Nitrogen-doped porous carbon nanosheets templated from g-C_3N_4 as metal-free electrocatalysts for efficient oxygen reduction reaction. *Adv. Mater.,* **2016**, *28*: 5080–5086.
[25] Buttersack C. Modeling of type IV and V sigmoidal adsorption isotherms. *Phys. Chem. Chem. Phys.,* **2019**, *21*: 5614–5626.
[26] Xiao M L, Xing Z H, Jin Z, et al. Preferentially engineering FeN_4 edge sites onto graphitic nanosheets for highly active and durable oxygen electrocatalysis in rechargeable Zn-Air batteries. *Adv. Mater.,* **2020**, *32*: 2004900.
[27] Fu X, Li N, Ren B, et al. Tailoring FeN_4 sites with edge enrichment for boosted oxygen reduction performance in proton exchange membrane fuel cell. *Adv. Energy. Mater.,* **2019**, *9*: 1803737.
[28] Li J K, Ghoshal S, Liang W T, et al. Structural and mechanistic basis for the high activity of Fe-N-C catalysts toward oxygen reduction. *Enegy. Environ. Sci.,* **2016**, *9*: 2418–2432.
[29] Novozhilova I V, Coppens P, Lee J, et al. Experimental and density functional theoretical investigations of linkage isomerism in six-coordinate $\{FeNO\}^6$ iron porphyrins with axial nitrosyl and nitro ligands. *J. Am. Chem. Soc.,* **2006**, *128*: 2093–2104.
[30] Tylus U, Jia Q Y, Strickland K, et al. Elucidating oxygen reduction active sites in pyrolyzed metal-nitrogen coordinated non-precious-metal electrocatalyst systems. *J. Phys. Chem. C,* **2014**, *118*: 8999–9008.
[31] Nie Y, Ding W, Wei Z D. Recent advancements of Pt-free catalysts for polymer electrolyte membrane fuel cells. *CIESC Journal,* **2015**, *66*: 3305–3318.
[32] Gu J, Hsu C S, Bai L C, et al. Atomically dispersed Fe^{3+} sites catalyze efficient CO_2 electroreduction to CO. *Science,* **2019**, *364*: 1091–1094.
[33] Zhang N, Zhou T P, Ge J K, et al. High-density planar-like Fe_2N_6 structure catalyzes efficient oxygen reduction. *Matter,* **2020**, *3*: 509–521.

DOI: 10.52396/JUSTC-2022-0143
JUSTC, **2023**, 53(3): 0304